B.E. Cremers and O.U. Velasco Fuentes

Chaotic Advection by Dipolar Vortices on a Topographic β-Plane

Abstract

Dipolar vortices on a topographic β-plane meander around lines of equal ambient vorticity (i.e. equal fluid depth). During this motion exchange of mass takes place between the interior and the exterior fluid of the dipole as well as between the two dipole halves. This exchange is caused by a variation of the distance between the vortices due to stretching and squeezing of the dipole as well as by a variation of the strength of the vortices due to conservation of potential vorticity. The exchange process is simulated using a point-vortex model. The amount of mass exchange and the residence time of fluid particles is evaluated using recent techniques for transport in dynamical systems.

Introduction

The basic dynamics of dipolar vortices on the β-plane can be understood using a point-vortex model, with the vortices' circulations changing in order to preserve potential vorticity (see e.g. Velasco Fuentes and van Heijst, 1994a, hereafter called VFvH). Using this approach, it is found that the motion of the couple displays three regimes: (i) eastward meandering, (ii) westward cycloid-like trajectories, and (iii) non-propagating, 8-shaped trajectory.

The gradient of the Coriolis parameter on the Earth can be mimicked in the laboratory by variations in the depth of a rotating fluid, when these variations are linear and small. This effect is usually referred to as the "topographic β-effect". On a topographic β-plane the direction of decreasing depth of the fluid corresponds to 'north'. VFvH studied analytically and experimentally the dynamics of dipolar vortices on a topographic β-plane. They found that the dipolar vortex meanders around isolines of ambient vorticity (i.e. lines of equal depth of the fluid), when the angle between the initial direction of the dipole and the 'east' direction is not zero. It is also observed that during this meandering motion fluid is exchanged between the dipole and the surroundings as well as between the two dipole halves.

In this particular case transport of fluid is dominated by a convective process so that the relative motions of fluid parcels is important. The study of particle motion ('Lagrangian' view) can be started if the velocity field of the flow

('Eulerian' view) is known for all times. Using the point-vortex approach, and given a particular set of initial conditions, the positions and strengths of the point vortices are known for all times. Therefore, the motion of individual particles, which is far more complex than the motion of the couple itself, can be extensively analysed using recent developments in the theory of transport in nonlinear dynamical systems (Wiggins, 1992). In particular, some of these methods can be used to calculate physically measurable quantities such as the amount of exchange across certain boundaries and the residence times of particles in chaotic regions of the flow. Rom-Kedar *et al.* (1990) used the latter approach to study chaotic particle motion due to a point-vortex dipole embedded in an an oscillating strain-rate field. This work should be consulted by readers interested in a detailed discussion of the techniques used in following sections.

Theory

The equations describing the trajectory of a fluid particle in an incompressible two-dimensional flow are

$$\frac{dx}{dt} = \frac{\partial \Psi}{\partial y} \qquad \frac{dy}{dt} = -\frac{\partial \Psi}{\partial x} \tag{1}$$

where Ψ is the stream function of the flow. This is a Hamiltonian system with Ψ playing the role of the Hamiltonian. If the flow is steady (Ψ time independent) particle motions are integrable, the trajectories being simply the streamlines. Time dependent flows, however, can produce chaotic particle trajectories, at least in some regions of the flow.

A dipolar vortex can be modelled, in a first approximation, by a couple of point vortices of (initially) equal but opposite strengths $\kappa_1 = 1$ and $\kappa_2 = -1$, separated by a constant distance $d = 1$. With dimensionless time defined as $t^* = t/2\pi$, the point vortices move along a straight line with a constant velocity $V_0 = 1$. The stream function of the flow induced by this unperturbed dipole (with the vortices in $y = \pm d/2$) in a frame moving with the structure is

$$\Psi = -\kappa_1 \ln(x^2 + (y - d/2)^2) - \kappa_2 \ln(x^2 + (y + d/2)^2) + C \tag{2}$$

where the correction term $C = -y$.

With the models introduced in the following section, it will be necessary to write $\Psi = \psi_u(x, y) + \varepsilon\psi_p(x, y, t)$ and to change C accordingly to obtain a stationary frame; here, ψ_u represents the unperturbed, steady state and ψ_p the time-periodic perturbation.

For time-periodic flows a significant simplification of the description of particle motion is achieved by using the Poincaré map —the map of the particle location $(x(t_0), y(t_0))$ to the location one period later $(x(t_0 + T), y(t_0 + T))$. For

$\varepsilon = 0$, a point and its mapping lie on the same streamline. There exist two fixed points p_+ and p_- corresponding to the front and rear stagnation points of the dipole, respectively. Both are of hyperbolic type so that there is a collection of orbits forming a line that approaches p_- as $t \to +\infty$, called the stable manifold, and a collection of orbits that emanates from p_+ (i.e. approaches p_+ as $t \to -\infty$), called the unstable manifold. In the unperturbed case the unstable manifold of p_+ and the stable manifold of p_- coincide and correspond to the separatrix (figure 1a).

For $\varepsilon \neq 0$ the fixed points persist and the unstable manifold of p_+ smoothly emanates from p_+ as before, but in this case undergoes strong oscillations as it approaches p_-. A fluid mechanical analogy illustrates the numerical computation of the unstable manifold: a circle of tracers is placed around the stagnation point and as times progresses the small circle will be stretched in the direction of the unstable manifold. The stable manifold is constructed in a similar way, but the integration now backwards in time.

The structure which results from the intersection of the manifolds of the two hyperbolic points is called a heteroclinic tangle (figure 1b). The intersecting manifolds create a mechanism for transport of fluid between the interior and the exterior of the vortex dipole in the following way. Note that the area ABCD in figure 1c maps to the area A'B'C'D'. This is because (i) the points A,B,C,D lie on (at least) one manifold and therefore they map to points on the same manifold; and (ii) the Poincaré map preserves orientation (see Wiggins, 1992). If the upper half of the trapped fluid is redefined as that enclosed by $p_+ C$ on the

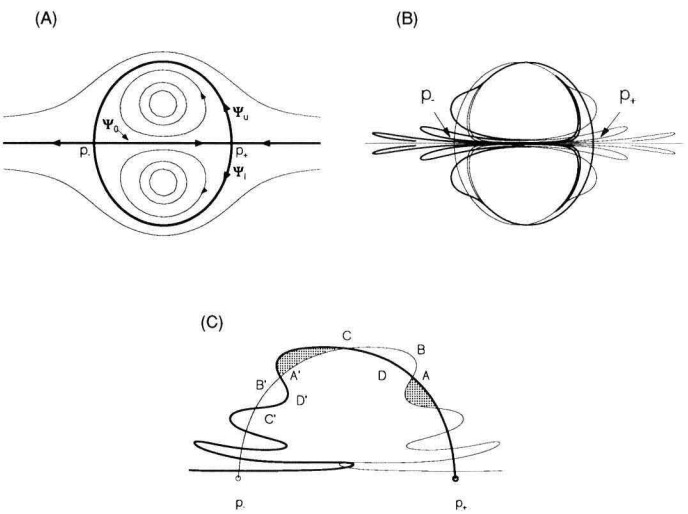

Fig. 1. (a) Streamlines of an unperturbed point-vortex dipole. (b) The heteroclinic tangle in the perturbed case. The thick line is the unstable manifold (the observable structure in flow visualization) and the thin line is the stable manifold. (c) The transport mechanism in the heteroclinic tangle. Region ABCD is mapped to A'B'C'D' (see text).

unstable manifold of p_+, and Cp_- on the stable manifold of p_- and p_+p_- on the x-axis, then the area ABCD represents the fluid that will be entrained in the next cycle. Similarly, the dotted area near A represents the fluid that will be detrained in the next cycle. Since the flow is incompressible, the area entrained is equal to the area detrained in every cycle.

The exchange of mass can be evaluated directly from the discrete set of points defining the manifolds. Once a single lobe is identified the area follows from $\mu = \int x\, dy$ along AB-BA. This method is valid for every amplitude of perturbation ε.

For small ε, one can obtain an $O(\varepsilon)$ approximation for the area of a lobe by using the Melnikov function (Rom-Kedar *et al.* 1990). The area of a lobe is given by

$$\mu = \varepsilon \int_{t_{01}}^{t_{02}} M(t_0)\, dt_0 + O(\varepsilon^2) \tag{3}$$

where t_{01} and t_{02} are two adjacent zeros of the Melnikov function $M(t_0)$ (i.e. they correspond to adjacent intersections of the unstable and stable manifolds). $M(t_0)$ is defined as

$$M(t_0) = \int_{-\infty}^{\infty} \| \vec{U}(\vec{x}_u(t)) \times \vec{u}(\vec{x}_u(t), t + t_0) \|\, dt \tag{4}$$

Here $\vec{U} = (\partial\psi_u/\partial y,\ -\partial\psi_u/\partial x)$ is the unperturbed flow; $\vec{u} = (\partial\psi_p/\partial y,\ -\partial\psi_p/\partial x)$ is the time-periodic perturbation; and $\|\cdot\|$ denotes the magnitude of a vector. The coordinates of points belonging to the unperturbed manifold $\vec{x}_u = (x_u(t), y_u(t))$ are expressed as a function of the parameter t.

Analytical and numerical results

Strengths perturbations

As described by e.g. VFvH, the evolution of a symmetric point-vortex dipole on the β-plane is governed by a second order ordinary differential equation for the dipole's direction of propagation. In the limit of small β-effect with respect to the vortex circulation ($\beta r L^2/\kappa_0 \ll 1$) and small initial deviation from eastward propagation ($\alpha_0 \to 0$), the following equations can be used for the vortex circulation (κ), the meridional position of the dipole's centre (ξ) and the direction of propagation (α)

$$\kappa_{1,2} = \pm 1 - \beta\xi \tag{5}$$

$$\frac{d\xi}{dt} = \alpha \tag{6}$$

$$\frac{d\alpha}{dt} = -2\beta\xi \tag{7}$$

Initial conditions are $\xi(0) = 0$, and $\alpha(0) = \alpha_0$. Therefore, the perturbation of the vortices' strengths is approximately given by:

$$\kappa_1(t) = 1 - \varepsilon_1 \sin \omega t \tag{8}$$

$$\kappa_2(t) = -1 - \varepsilon_1 \sin \omega t \tag{9}$$

where $\varepsilon_1 = \alpha_0 \sqrt{\beta/2}$, and $\omega = \sqrt{2\beta}$.

Because of the varying asymmetry of the vortices, the vortex pair neither moves along a straight line nor rotates around a fixed point. The motion of the vortex can be described as a rotation with varying angular speed $\Omega(t) = -2\varepsilon_1 \sin \omega t$ around a point lying on the line defined by the two point vortices and located at a varying distance $R(t) = (\varepsilon_1 \sin \omega t)^{-1/2}$ from the dipole's centre. A steady stream function results from substitution of κ_1, κ_2 and the correction term $C = \Omega(t)[x^2 + (y - R(t))^2]/2$ in (2).

Because of the asymmetries present in the dipolar flow structure not only the outer manifolds, but also the middle manifold will break up. As a consequence, besides entrainment and detrainment of fluid, exchange of mass between the two dipole halves will occur.

Two dimensionless parameters characterize the perturbation: the perturbation amplitude ε_1 and the ratio between the (dimensionless) perturbation period

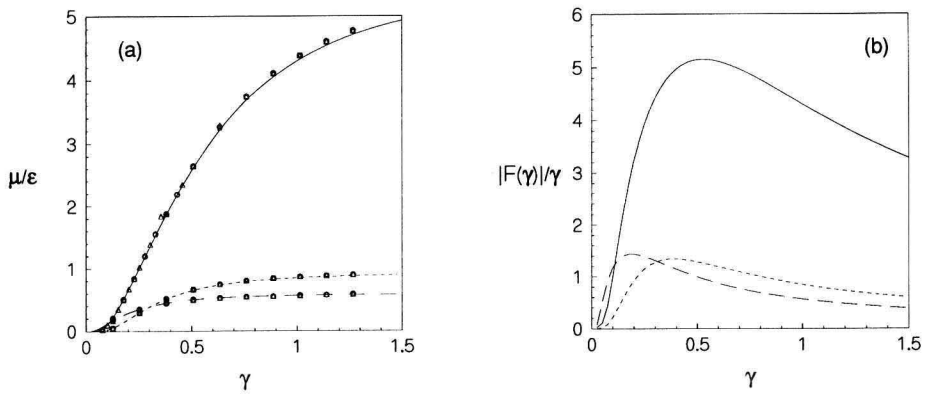

Fig. 2. Transport in the perturbed point-vortex dipole: (a) lobe area μ (normalized by the perturbation amplitude ε), and (b) exchange rate $\mu^* = F(\gamma)/\gamma$ as a function of γ. The lines indicate the Melnikov function calculations, and the markers denote results from direct numerical integration of the advection equations.

$T = \omega^{-1}$ and a timescale associated with the dipole's translation d/V. The latter parameter is defined to be $\gamma = (2\beta)^{-1/2}$.

The lobe area according to the Melnikov function is $\mu = \varepsilon_1 F(\gamma) + O(\varepsilon_1^2)$, where $F(\gamma)$ is the numerically computed function shown in figure 2a. The dotted line represents the exchange of mass between interior and exterior and the broken line exchange between the dipole's halves. In the same figure the markers show the lobe areas evaluated by direct numerical integration for $\varepsilon_1 = 0.01$, 0.05 and 0.1.

Size perturbations

The meandering trajectory of a dipolar vortex on a topographic β-plane causes the water column to be alternatingly stretched and squeezed. As a result the distance between the vortex centres will decrease as the dipole moves into deep water and increase as the dipole moves towards shallower water. This effect is modelled using the same point-vortex dipole but imposing on it a sine-like variation of the distance between the vortices: $d = d_0(1 + \varepsilon_2 \cos \omega t)$. The point vortices have constant circulation κ_0 and $-\kappa_0$, respectively. Because of symmetry about the x-axis the middle manifold remains unaffected and no exchange of fluid can occur between the two halves of the vortex dipole.

In figure 2a the solid line represents the absolute value of the function $F(\gamma)$ obtained with the Melnikov function and the markers show the lobe areas (divided by the perturbation amplitude) obtained from direct numerical integration of the advection equations for $\varepsilon_2 = 0.01$, 0.05 and 0.1.

Perturbation of the dipole's size produces stronger entrainment/detrainment than perturbation of the strengths. For strength perturbation, the exchange of fluid between the two halves of the vortex pair is more than the exchange of fluid between the interior and the exterior of the vortex pair up to $\gamma = 0.3$. For greater values of γ, the relation is reversed. For all three ways of exchange of fluid, the function $F(\gamma)$ increases with γ. This can be understood because a larger period allows for more fluid to be exchanged. However, this behaviour changes for the exchange rate (mass exchanged per unit of time). As can be seen in figure 2b, the exchange rate is maximal where $F(\gamma)/\gamma$ is maximal. In the case of size perturbation, we found this to occur for $\gamma = 0.528 \pm 0.001$. For strength perturbation, the exchange rate between interior and exterior fluid is maximal for $\gamma = 0.386 \pm 0.001$ and the exchange rate between the two halves of the vortex pair is maximal for $\gamma = 0.189 \pm 0.001$.

Particle transport

All fluid detrained during the first cycle is originally "interior fluid"; this is, however, not necessarily the case for later cycles. Some of the detrained fluid will be "exterior fluid": fluid parcels originally located outside the dipole, later being entrained and finally, after a few cycles are returned to the surroundings.

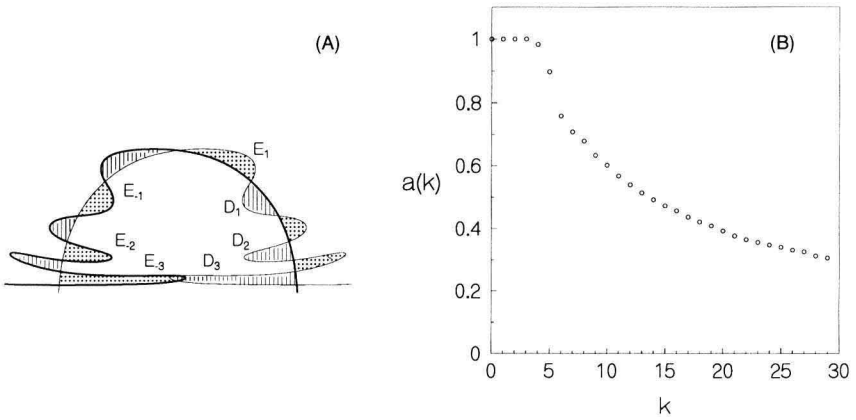

Fig. 3. (a) Intersection of detrainment (D_3) and entrainment lobes (E_{-3}) provides information about residence times and transport of species (see text) (b) Fraction a of the detrainment lobe formed by "interior fluid", as a function of the number of perturbation cycles k.

The determination of the amount of interior fluid that is detrained in cycle k is highly simplified by the knowledge of the lobe geometry. In particular by the intersections of the entrainment (E) and detrainment (D) lobes, as shown in figure 3a. A positive subindex indicates in which cycle, forward in time, the lobe will change the region; a negative subindex indicates the cycle, backwards in time, in which the lobe changed of region. The intersection of E_{-3} and D_3 that will be detrained during the third cycle represents fluid that was located outside the dipole three cycles before. Thus in general $D_i - D_i \cap E_{-j}$ gives the area of interior fluid that escapes the dipole in the $k = i + j$ period of the perturbation. In figure 3b the fraction of interior fluid that is detrained after k cycles is shown for the case $\varepsilon_2 = 0.1$ and $\kappa = 0.15$.

Experiment

For comparison, laboratory observations and a numerical simulation that matches the parameters used in the experiment are shown. For details on the experimental technique see VFvH. The experimental parameters are: period of the rotating table $T = 11$ s; fluid depth $h_0 = 18$ cm; and gradient of the sloping bottom is 0.04. With these parameters the topographic β-effect measured $\beta = 0.247\ \mathrm{m}^{-1}\,\mathrm{s}^{-1}$ (see VFvH). In this experiment the dipole was started at an angle $\alpha_0 = \pi/4$. The angular frequency of the perturbations and the amplitude of strength perturbation can be computed directly from the experimental parameters: $\varepsilon_1 = \alpha_0 \sqrt{\beta/2}$, $\gamma = (2\beta)^{-1/2}$; and the amplitude of the size perturbation is measured directly from the experiment, yielding $\varepsilon_2 = 0.1$.

Three stages in the dipole's evolution are shown in figure 4. One lobe has been formed when the dipole reaches its northermost position (figure 4a) by detrainment of fluid from the negative half (upper side in the picture). A second lobe

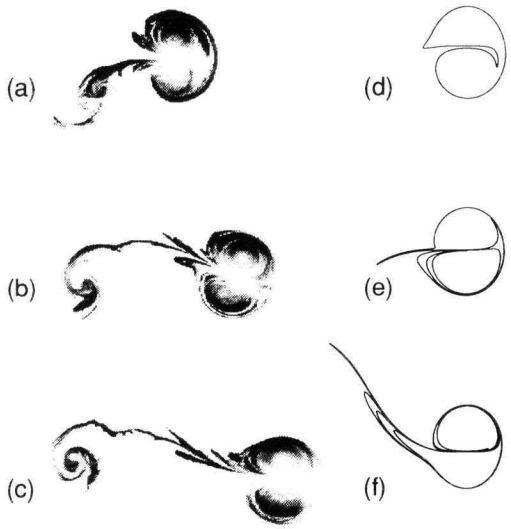

Fig. 4. The formation of lobe-like structures in the fluid transported by a dipolar vortex on a topographic β-plane. Experimental images (a)-(c) and numerical calculations (d)-(f) are shown at T/4, T/2 and 3T/4 , with T the period of the dipole's oscillatory motion.

is formed on the negative half when the dipole returns to its equilibrium position (figure 4b). Both lobes are stretched along the tail (figure 4c).

The deformation of the patch of dye is simulated numerically by following the evolution of the initial separatrix. In figure 4d–4f we can see the deformation of the separatrix in a frame moving with the vortex pair at stages corresponding with the experimental figures. While the distance between the two vortices increases and the negative vortex becomes stronger, fluid is entrained into the dipole and begins to circle around the negative vortex (figure 4d). Detrained fluid is left behind from the positive half of the vortex dipole and forms a long tail. After this stage fluid is also entrained into the positive vortex (figure 4e) and fluid is detrained from the negative half, forming a second lobe (figure 4f).

Qualitatively, similar features can be recognized such as entrainment and detrainment of fluid and the associated formation of lobes. Note that the long tail in the experiment is formed during the generation of the dipolar vortex and is not primarily a result of fluid detrainment. In general, not all the dye lies initially within the vortex (see VFvH). In the numerical simulation, however, the advected line corresponds with the original separatrix.

Conclusions

The exchange of fluid induced by a dipolar vortex on a topographic β-plane is investigated. The dipole meanders around lines of equal ambient vorticity if

it initially travels transversally to those lines. During the meandering, the dipole shows a variation in size (due to squeezing and stretching as the dipole moves between the shallow and deep sides of the tank) and a variation in the intensity of the individual vortices (due to conservation of potential vorticity). Consequently there is a continuous exchange of mass between the interior and the exterior fluid of the dipolar vortex, and between the two dipole halves.

The two exchange mechanisms have been studied independently using a point-vortex model, which has been shown to describe reasonably well the meandering of the dipole (see VFvH). The exchange of fluid due to the strengths perturbation is studied in the linear limit (α_0 small) of the modulated point-vortex dipole and the effect of size perturbation is studied by prescribing a periodic variation of the distance between the point vortices.

Recent developments in the theory of transport in dynamical systems (lobe dynamics, see Rom-Kedar *et al.* 1990) have been applied to these particular problems. For small amplitudes of perturbation the area of a lobe evaluated using direct numerical integration corresponds well with the results obtained using the Melnikov function.

For equal amplitudes of perturbation (i.e. the same percentual variation with respect to the unperturbed value), the size variation causes more exchange of fluid than the variation of strength.

Although the total exchange of fluid increases with increasing perturbation period, the exchange rate shows a maximum for a specific value of the period of perturbation. This value is different for each mass exchange mechanism.

The analysis of the transport of species (particles with a particular origin, e.g. interior or exterior regions of the dipole) is simplified by the knowledge of the lobe geometry. For a specific set of parameters, this is illustrated by the computation of the fraction of detrained fluid that was originally within the dipole.

Numerical simulations of the deformation of the separatrix using size and strength perturbation is compared with laboratory observations of dye patterns produced by a dipolar vortex on a topographic β-plane. Good qualitative agreement exists. The observed differences are likely due to: (i) the discrete representation of the original vorticity distribution (ii) the absence in the model of relative vorticity generated by advection of ambient fluid.

Acknowledgement

O.U.V.F. gratefully acknowledges financial support from the Stichting voor Fundamenteel Onderzoek der Materie (FOM).

References

Rom-Kedar, V., A. Leonard, and S. Wiggins, 1990 - An analytical study of transport, mixing and chaos in an unsteady vortical flow. *J. Fluid Mech.* **214**, 347–394.

Velasco Fuentes, O.U. and G.J.F. van Heijst, 1994a - Experimental study of dipolar vortices on a topographic β-plane. *J. Fluid Mech.* **259**, 79–106. See also: Velasco Fuentes, O.U. and G.J.F. van Heijst, 1994b Laboratory experiments on dipolar vortices in a rotating fluid. This issue.
Wiggins, S., 1992 - *Chaotic Transport in Dynamical Systems.* Springer.

Fluid Dynamics Laboratory
Eindhoven University of Technology
P.O. Box 513
5600 MB Eindhoven
The Netherlands